# Taking Traction Control to Task

*High-Adhesion-Point Tracking Based on a Disturbance Observer in Railway Vehicles*

LIJUN DIAO, LEITING ZHAO, ZHEMING JIN, LEI WANG, AND SULEIMAN M. SHARKH



Railway vehicles have been based on a wheel-rail system since the system's origination. Therefore, the adhesion-coupling behavior between wheel and rail is the fundamental element of railway traction [1]. However, low vehicle wheel-rail adhesion caused by high humidity, rain, snow, oil, or decomposing leaves is a common problem that can cause damage to some elements of the traction system and decrease traction performance [2]. It may even give rise to safety problems and reduce comfort, not to mention delays and their corresponding economic impact. Good traction control to ensure the system is working at high adhesion point is therefore critical and mandatory for the traction control units (TCUs) [2]–[6].

In modern railway vehicles, a typical adhesion control system calculates the speeds of traction motors and trailer wheels, and the reference speed is set to a minimum speed among the components in the powering mode or the maximum speed in the braking mode. The TCU calculates the speed difference between the motored truck and the reference speed, and the tractive effort of the traction motors is reduced as soon as the speed difference exceeds a certain value, until the slip or slide ceases. With this method, we can achieve a high tractive force.

The traction control of adhesion force is based on three fundamental pillars: speed measurement, traction motor control, and adhesion control. However, the number of pulses per rotation of the speed sensor is normally much smaller than that widely used in other industrial applications [7], so the level of accuracy of speed measurement using a basic pulse count is

*Digital Object Identifier 10.1109/MIE.2016.2644699*
*Date of publication: 21 March 2017*

**The traction control of adhesion force is based on three fundamental pillars: speed measurement, traction motor control, and adhesion control.**

not usually sufficient. To improve the accuracy, a field-programmable gate array with a digital filter, a high-speed clock, and a parallel algorithm can be used in speed measurement.

Good motor control is essential to realizing good vehicle dynamic performance [8]; when slippage or sliding occurs, the tractive force is reduced by the motor controller automatically, the more the better. However, the acceleration of the vehicle will be reduced correspondingly, resulting in exceeding the running time constraints. Thus, it is the responsibility of the adhesion controller to maintain good tractive performance within the acceptable slip range.

To achieve this, we have to learn how the tractive force is transmitted in the traction system and what will happen on the wheel-rail contact surface. Innovative adhesion models considering the wheel-rail contact surface, which increase the control accuracy by reproducing degraded adhesion conditions in vehicle dynamics and railway systems, are described in [9]–[11]. However, such goals are not easy to achieve due to nonlinearities and uncertainties associated with wheel-rail surface conditions, train speed, and operating conditions [2].

In this article, a comparative study of adhesion control methods in different railways is made, including rubber-tire and steel-wheel types used in urban and mainline railways. The steel-wheel type of urban railway is chosen as a study case in this research, as the adhesion control methods of all these types are similar. The state-of-the-art of adhesion research is then discussed.

A control strategy using a first-order disturbance observer is proposed to realize better adhesion control performance on the basis of wheel-rail adhesion characteristics and a simplified equivalent single-axle model. An additional dynamic torque tuning function is used to adjust the torque slightly to maintain the robust performance of adhesion control. Finally, the torque reference given by the general vehicle logic controller is combined with the proposed adhesion control and used to control the traction motors on the basis of a field-oriented control (FOC) strategy. Simulations and experiments were carried out to validate the control strategy. The proposed adhesion method can also be extended to other types of railway vehicles, such as mainline railways or rubber-tire trains.

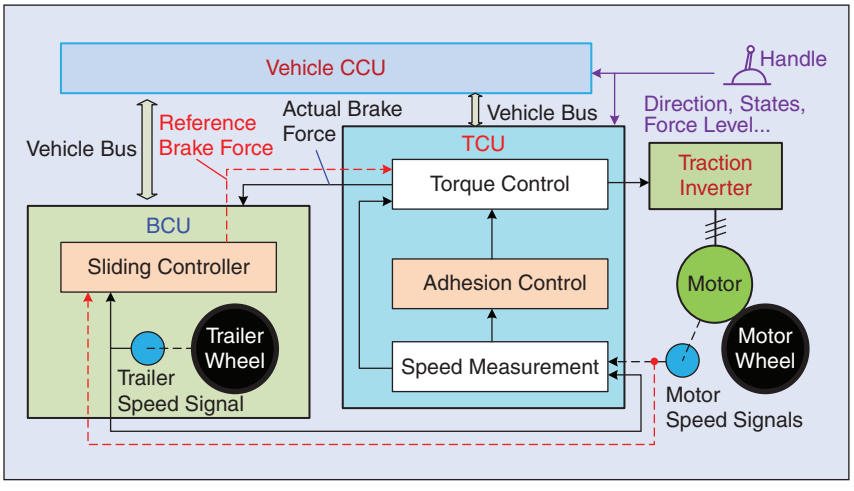


FIGURE 1 – A general diagram of adhesion control for traction systems.

## Adhesion Control Application and Research

We first compare the adhesion control application differences between rubber-tire and steel-wheel trains. Rubber-tire trains have advantages of greater adhesion and better acceleration in operation [12]; however, modern steel-wheel trains using distributed traction with a high proportion of powered axles have narrowed the adhesion performance gap compared to rubber-tire trains. Additionally, rubber-tire trains have similar traction logic and motor controls compared to those used in steel-wheel controls, which means that even though the adhesion characteristics are quite different, the adhesion control algorithm is similar [13]–[15].

Then we discuss the adhesion control differences between urban railways and mainline railways. In urban railways, the control is fulfilled through cooperation among the central control unit (CCU), the brake control unit (BCU), and the TCU. The general adhesion control diagram is shown in Figure 1. Generally, the TCU receives traction orders from the cab handle directly or from the CCU through the vehicle communication bus and then applies adhesion control to motor axles. The BCU regulates its mechanical braking force when sliding happens during the braking state. Of course, the BCU will always compensate the total braking force according to the actual electric braking force feedback from the TCU. The difference in mainline railways, especially electric multiple units using distributed traction, is that the BCU completes the braking slide algorithm for the motor axles instead and then sends the final reference of braking force to the TCU, which, by this point, just has to perform traction slip control. Another major difference in the operating pattern between urban railways and mainline railways is that urban railways normally require much more frequent starts and stops as the distances between stations are much shorter and the acceleration is much higher.

Therefore, the wheel slip/slide normally imposes a greater problem when compared with mainline services. The

adhesion control theory for urban and mainline railways remains quite similar, however, and it is very easy to transplant the algorithm from one to the other by changing the cooperation logic between the BCU and the TCU. Without loss of generality, this article mainly discusses adhesion control strategies of steel-wheel trains, especially those used in urban railways. Figure 2 summarizes different adhesion control approaches, each of which can be used to achieve a relatively ideal adhesion coefficient. The frequently proposed adhesion control schemes in the literature are based on conventional configurations with reference speed or on acceleration without a reference speed [1], [16]–[18], which are relatively simple and can achieve relatively high adhesion efficiency. According to [16], the actual adhesion coefficient can be improved, and the acceleration time can be shortened by 8% compared with an early control method. In [7], the derivative of motor current was utilized in place of the speed information for wheel slip detection of a multiple motor drive system, but additional current sensors are needed. The conventional control strategies given previously can be simply realized, and they have fast responses and low risk. When slippage or sliding occurs, however, the torque needs to be reduced quickly and then increased slowly to prevent slipping from occurring again. The adhesion point is often far away from the peak value, and adhesion efficiency is relatively low.

To overcome these shortcomings, many scholars have proposed other adhesion control strategies [19]–[24]. For example, the slip velocity method in [20] is relatively simple and intuitive, but the precise measurement of slip velocity is not an easy task. The ordinary adhesion derivative method in [21] directly calculates the differential adhesion coefficient as a function of time, which causes noise to be amplified and increases the vulnerability of the control systems.

There are also some adhesion strategies based on intelligent control theories. The fuzzy logic–based control strategy described in [25] outputs the optimal slip velocity reference according to preestablished fuzzy rules and thus regulates the motor torque via a proportional integral (PI) controller. In [26], a wavelet denoising method is used to identify slip tendency, and the torque command is tuned by a cloud model. However, these intelligent rules require large amounts of data and computation, which makes robust software programming difficult and limits their application in rail transit, where high reliability, security, and real-time performance are needed. In contrast, the adhesion control strategy based on a model control law is simple and easy to apply because there is no need to calculate the slip velocity and the system is always working near the peak adhesion point by real-time adjustments of the motor torque; the only consideration is that the derivative of the current wheel-rail peak adhesion coefficient must be zero [27], [28].

Based on the model control, [29] proposes an antislip control system based on the ordinary disturbance observer, which is called a zero-order disturbance observer. It is simple, easy to realize, and has a good antislip response. However, the inputs and variables of a zero-order disturbance observer are susceptible to interference by electromagnetic noise. Therefore, in the case of large variations of the adhesion force coefficient, it is sometimes difficult to keep the adhesion control reference near to the maximum adhesion force. To overcome this problem, [30] proposes an adhesion control method with a full-dimension state observer, which introduces a feedback correction path in the adjustment of the state variables. However, the zero-order disturbance observer and full-dimension state observer cannot directly obtain the load torque derivative values, which require additional derivative computing that will amplify noise and make the control system vulnerable to interference. In this study, we will use a first-order disturbance observer combined with a dynamic torque tuning function to compensate for the aforementioned shortcomings.

**The adhesion behavior of steel-wheel railways is determined by the forces arising between two surfaces in contact, where a phenomenon called *creepage* will occur.**

## Vehicle Adhesion Characteristics and Dynamic Model

### *Wheel-Rail Adhesion Characteristics*

The adhesion behavior of steel-wheel railways is determined by the forces arising between two surfaces in contact,

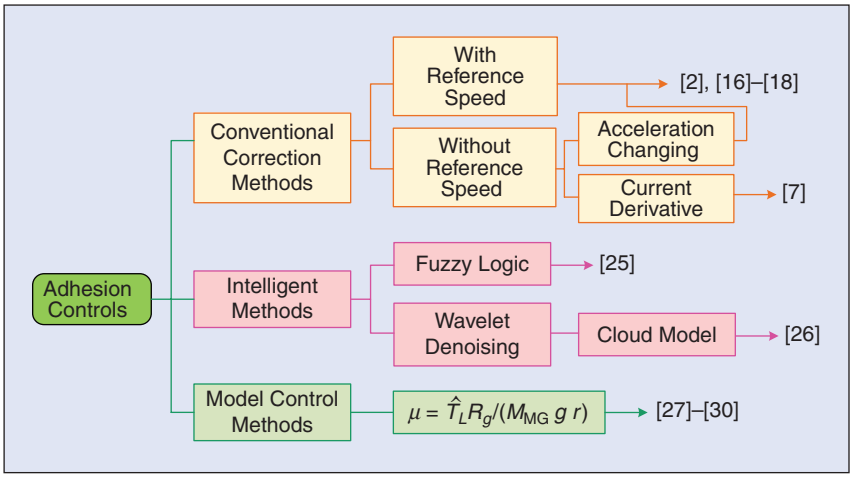


FIGURE 2 – A summary of the different adhesion control approaches.

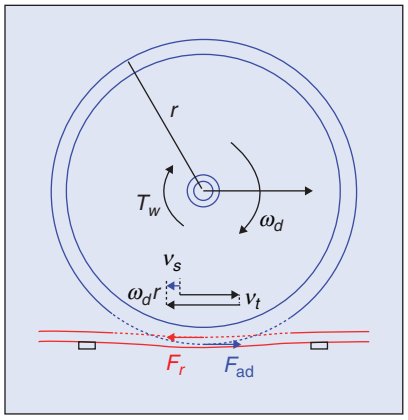


FIGURE 3 – An illustration of the creepage phenomenon.

where a phenomenon called *creepage* will occur. This phenomenon can be defined as a wheel-rail micro-elastic slide through relative deformation as shown in Figure 3 [1]: when a tractive force (torque $T_w$) is applied on a railway wheel, a small difference arises between the forward velocity $v_t$ and wheel circumference line velocity $v_d$ (circumferential angular velocity $\omega_d$). The relative difference is the creepage. It is resisted by the friction force $F_{ad}$ on the wheel with radius $r$. The result slip velocity $v_s$ can be defined as

$$\begin{cases} v_s = v_d - v_t \\ v_d = \omega_d r. \end{cases} \tag{1}$$

To design the adhesion control system, the adhesion characteristics must be considered as exactly as possible by using the adhesion coefficient $\mu$, which is usually defined as the ratio between the wheel-rail tangential force (or adhesion force) $F_{ad}$ and the normal force $F_G$ on the wheel. The definition shows that, when the load is constant, the available $F_{ad}$ is proportional to $\mu$

$$\mu = \frac{F_{ad}}{F_G}. \tag{2}$$

The fundamental relationship between the average value of $\mu$ and wheel slip under different rail conditions is shown in Figure 4 [17], [32]. It can be seen that a dry, clean wheel-rail surface condition will have a high $\mu$, but a wet surface under rainy, snowy, foggy, or frosty weather conditions will have a much lower $\mu$; $\mu$ will be further reduced when the surface is oily. However, the different characteristic curves have their own peak adhesive point at a slip velocity $v_{spot}$. The adhesion system will be stable when the slip velocity is less than $v_{spot}$, and $\mu$ increases nearly linearly with the slip velocity. However, when the slip velocity is greater than $v_{spot}$, $\mu$ decreases rapidly when the slip velocity increases, and the system will be unstable.

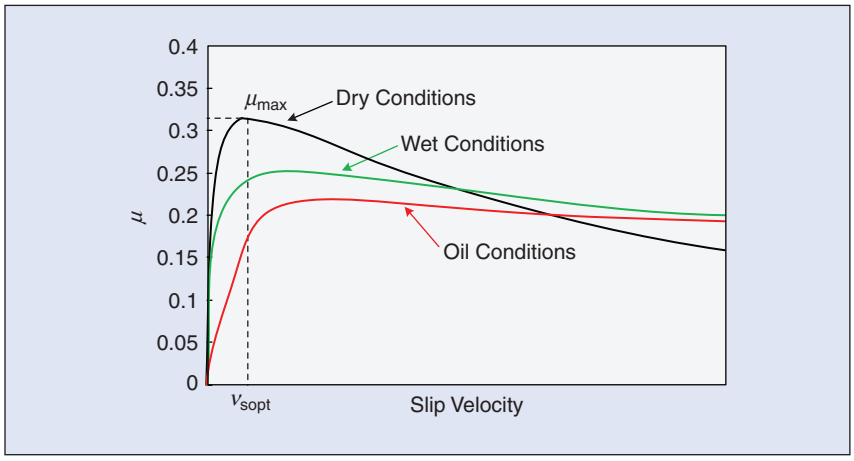


FIGURE 4 – Adhesion characteristic curves under different rail surface conditions.

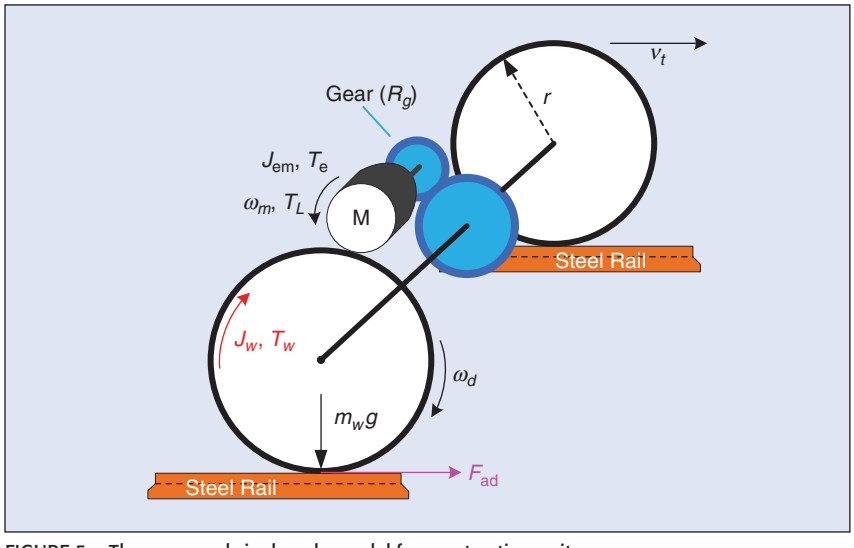


FIGURE 5 – The proposed single-axle model for one traction unit.

### *Vehicle Dynamic Model*

To study the adhesion characteristics of the wheel-rail surface from the electric control perspective, it is necessary to establish a model that can reflect the relationship between electric control and adhesion characteristics. An accurate physical model considering all the dynamics of the entire vehicle, such as longitudinal, lateral, and vertical dynamics, would therefore be ideal. It is very difficult to capture all the dynamics, however, because of the complex and nonlinear behavior of the adhesion coefficient, as well as the external unknown contaminants that are present between the contact surfaces [9]. Additionally, most traction systems consist of one or several traction units, where the wheels in the same bogie or even different bogies are driven by motors connected in parallel and powered by the same traction converter. The differences of motor parameters, wheel diameters, weight on each axle, etc. will make an accurate model of a traction unit much more complicated.

We have focused primarily on the adhesion control itself, so many other factors will not be discussed in this article. A simplified one-dimensional single-axle model as shown in Figure 5 is proposed

in the analysis, which can be used to synthetically reflect the essential characteristics of one traction unit [29]. The single-axle model makes the following assumptions for its traction unit:

- The parallel motors have exactly the same characteristics and time-variant parameters. The diameter differences of the wheels are small enough to be neglected [33], [34].
- The mass is distributed equally on each motor axle. The transmission losses in the gears are also neglected.
- At every time interval, the rail condition for each wheel is the same, and the elastic deformation of the wheel-rail surfaces is quite similar.

In the model shown in Figure 5, the motor is powered by the traction converter, and the tractive force is transmitted from the motor to the wheels through a gearbox. The equivalent wheel and motor rotation equations of the model can be written as

$$\begin{cases} F_{\text{ad}} = \mu m_w g \\ J_w \dfrac{d\omega_d}{dt} = T_w - F_{\text{ad}} r \\ T_w = T_e R_g \\ T_L = F_{\text{ad}} r / R_g \\ J_{\text{em}} \dfrac{d\omega_m}{dt} = T_e - T_L, \end{cases} \tag{3}$$

where $g$ is the gravitational acceleration constant; $R_g$ is the gear transmission ratio; $\omega_m$, $T_e$, and $T_L$ are the mechanical angular speed, total electromagnetic torque, and equivalent load torque of the traction motor, respectively; $J_{\text{em}}$ and $J_w$ are the total equivalent motor torque inertia and total equivalent wheel moment inertia, respectively; $m_w$ is the total mass put on the motor axles of the traction unit; $m_w = (m_M + m_L)/N_c$; $m_M$ and $m_T$ are the dead mass of a powered carriage and a trailer carriage, respectively; $m_L$ is the average load mass of each carriage; and $N_c$ is the number of traction units for each powered carriage.

The motion equation of the whole train can be written as

$$\sum_{i=1}^{(N_c \times N_{\text{mc}})} F_{\text{adi}} - F_R = [N_{\text{mc}}(m_M + m_L) + N_{\text{tc}}(m_T + m_L)] \frac{dv_t}{dt}, \tag{4}$$

where $F_{\text{adi}}$ represents the total adhesive force provided by number $i$ traction units; $F_R$ is the total resistance, including running resistance and slope resistance; and $N_{\text{mc}}$ and $N_{\text{tc}}$ denote the numbers of motored carriages and trailer carriages, respectively.

## Adhesion Control Based on High Adhesion Utilization

The slope of the adhesion characteristic curve can be deduced from Figure 4 as

$$\frac{d\mu}{dv_s} = \frac{d\mu/dt}{dv_s/dt} = \frac{\dot{\mu}}{\dot{v}_s}. \tag{5}$$

The slope will be either greater than zero when the system's operating point is on the left side of the adhesion characteristic curve or less than zero when it is on the right side. Otherwise, it approximately equals zero in the vicinity of the peak point. Meanwhile, the slip velocity of the vehicle is always changing due to the ever-changing powering or braking conditions, i.e., its derivative value is not zero. Thus, a search for the adhesion coefficient's peak point can be directly performed using the condition that $\dot{\mu} = 0$.

Among uncertainties of adhesion control, the adhesion coefficient is one of the most difficult variables to predict or measure directly, especially under changing wheel-rail surface conditions when the train is running. Beam-and-bristle models were developed to investigate adhesion coefficient characteristics and verify them experimentally [35]. It is difficult to build such complicated test rigs, however, and there are also various inherent differences among simulations, labs, and reality. This study will use other parameters that can be detected by the TCU itself to indirectly calculate or be equivalent to $\mu$.

### *Design of a First-Order Disturbance Observer*

According to (3), the adhesion coefficient $\mu$ is proportional to the equivalent motor load torque, $T_L$. However, the traction control system cannot detect the load torque of the motor in real time, i.e., during the actual running state. Therefore, a state observer needs to be used by reconstructing the current equivalent motor load torque according to input variables or variables that can be measured directly [26].

Traction motors drive rail vehicles by transmitting torque to the heavy wheels through gears, and the mechanical inertia of the whole vehicle is enormous. Hence, the equivalent load torque of the motors can be considered to be changing at a constant speed during a short calculation period, i.e., $\dot{T}_L$ is constant. Using $T_L$ and its derivative as state variables, a first-order disturbance observer of the linear state space is described in (6) in the box at the bottom of the page.

In (6), A, B, and C are coefficient matrices and $x$ is the state matrix of the model. The equivalent motor electromagnetic torque $T_e$ is the input variable, and $y = \omega_m$ is the output variable, which can be directly measured.

Define $\tilde{x}_1 = [\omega_m]$, $\tilde{x}_2 = [\dot{T}_L \;\; T_L]^T$; then, (6) can be rewritten as

$$\begin{bmatrix} \dot{\tilde{x}}_1 \\ \dot{\tilde{x}}_2 \end{bmatrix} = \begin{bmatrix} \tilde{\text{A}}_{11} & \tilde{\text{A}}_{12} \\ \tilde{\text{A}}_{21} & \tilde{\text{A}}_{22} \end{bmatrix} \begin{bmatrix} \tilde{x}_1 \\ \tilde{x}_2 \end{bmatrix} + \begin{bmatrix} \tilde{\text{B}}_1 \\ \tilde{\text{B}}_2 \end{bmatrix} T_e, \tag{7}$$

where the coefficient matrices with ~ symbols are derived from A or B in (6) separated by dotted lines.

If a state space for variable $\tilde{x}_2$ is defined as

$$\begin{cases} \dot{\tilde{x}}_2 = \tilde{\text{A}}_{22} \tilde{x}_2 + \tilde{u} \\ \tilde{y} = \tilde{\text{A}}_{12} \tilde{x}_2, \end{cases} \tag{8}$$

then combining (7) and (8) yields

$$\begin{cases} \tilde{u} = \tilde{\text{A}}_{21} \tilde{x}_1 + \tilde{\text{B}}_2 T_e \\ \tilde{y} = \dot{\tilde{x}}_1 - \tilde{\text{A}}_{11} \tilde{x}_1 - \tilde{\text{B}}_1 T_e. \end{cases} \tag{9}$$

$$\begin{cases} \underbrace{\begin{bmatrix} \dot{\omega}_m \\ \ddot{T}_L \\ \dot{T}_L \end{bmatrix}}_{\dot{x}} = \underbrace{\left[\begin{array}{c:cc} 0 & 0 & -1/J_{\text{em}} \\ \hdashline 0 & 0 & 0 \\ 0 & 1 & 0 \end{array}\right]}_{\text{A}} \underbrace{\begin{bmatrix} \omega_m \\ \dot{T}_L \\ T_L \end{bmatrix}}_{x} + \underbrace{\begin{bmatrix} 1 + J_{\text{em}} \\ 0 \\ 0 \end{bmatrix}}_{\text{B}} T_e \\ y = \underbrace{[1\;0\;0]}_{\text{C}} \underbrace{\begin{bmatrix} \omega_m \\ \dot{T}_L \\ T_L \end{bmatrix}}_{x}, \end{cases} \tag{6}$$

**TABLE 1 – VEHICLE AND CONTROL PARAMETERS.**

| SYMBOL | VALUE | SYMBOL | VALUE |
|---|---|---|---|
| $R_g$ | 6.37 | $m_T$ | 34 t |
| $r$ | 805 mm | $m_M$ | 38 t |
| $J_{em}$ | 5 kg.m$^2$ | $m_L$ | 25 t |
| $\mu_{cal}$ | 0.16 | $T_{ad-C1}$ | 0.15 $T_{ref}$ |
| $l_1, l_2$ | −150 | $T_{ad-C2}$ | 0.25 $T_{ref}$ |

From (6) and (7), it is obvious that the eigenvalues of the matrix $\tilde{A}_{22}$ are $\lambda_1 = \lambda_2 = 0$; thus, the linear system given in (8) is unstable. Therefore, use $L$ as the feedback gain matrix to construct a closed-loop state observer as

$$\begin{cases} \dot{\hat{x}}_2 = \tilde{A}_{22}\hat{\tilde{x}}_2 + \tilde{u} + L(\tilde{y} - \tilde{A}_{12}\hat{\tilde{x}}_2) \\ \quad = (\tilde{A}_{22} - L\tilde{A}_{12})\dot{\hat{x}}_2 + Lu\tilde{y} + \tilde{u} \\ L = [l_1 \;\; l_2]^T, \end{cases} \tag{10}$$

where ^ indicates the observed quantities.

Considering the tradeoff between different performance objectives, such as dynamic response and noise sensitivity, a reasonable choice of the values of the feedback gain matrix coefficients, $l_1$, $l_2$, can be selected to ensure the observer's stability, where the real parts of the eigenvalues for the system matrix $\tilde{A}_{22} - L\tilde{A}_{12}$ are negative.

However, (9) shows that the calculation of $\tilde{y}$ includes a derivative operation of $y = \tilde{x}_1 = \omega_m$, which will amplify high-frequency noise in $\tilde{y}$. It therefore leads to a direct impact on the accuracy of the observation results and the stability of the control system. To avoid this, define an intermediate state variable

$$z = [z_1 \;\; z_2]^T \text{ and}$$
$$z = \hat{\tilde{x}}_2 - Ly. \tag{11}$$

Taking the derivative of both sides of (11), and substituting (9) and (10) yields

$$\begin{aligned} \dot{z} &= \dot{\hat{\tilde{x}}}_2 - L\dot{\tilde{x}}_1 \\ &= (\tilde{A}_{22} - L\tilde{A}_{12})\hat{\tilde{x}}_2 + L\tilde{y} \\ &\quad + \tilde{u} - L(\tilde{y} + \tilde{A}_{11}y + \tilde{B}_1 T_e) \\ &= (\tilde{A}_{22} - L\tilde{A}_{12})(z + Ly) \\ &\quad + (\tilde{A}_{21} - L\tilde{A}_{11})y + (\tilde{B}_2 - L\tilde{B}_1)T_e \\ &= (\tilde{A}_{22} - L\tilde{A}_{12})z + [(\tilde{A}_{21} - L\tilde{A}_{11}) \\ &\quad + (\tilde{A}_{22} - L\tilde{A}_{12})L]y + (\tilde{B}_2 - L\tilde{B}_1)T_e. \end{aligned} \tag{12}$$

Substituting the coefficient matrices in (6) and (10) into (12), the final model of the first-order disturbance observer can be derived as shown in (13) at the bottom of the page.

As shown in (3), adhesion coefficient $\mu$ can be directly calculated using the observed value $\hat{T}_L$ by $\mu = \hat{T}_L R_g/(m_w g r)$, i.e., $\mu$ can be derived from (13). To assess the observer's performance with different values of the feedback gain matrix coefficients, simulations of changing wheel-rail surface conditions are carried out with different sets of $l_1$, $l_2$ and other parameters given in Table 1.

The results are shown in Figure 6, in which the load torque and its derivative values have been changed to $\mu$ and its derivative, $\dot{\mu}$. Figure 6(a) with $l_1 = l_2 = -30$ shows that the observed values have small steady-state errors but the dynamic response is slow, which makes the adhesion response not fast enough when the wheel-rail surface condition changes suddenly. But in Figure 6(b) with $l_1 = l_2 = -150$, the dynamic response becomes faster, which can meet the requirement of dynamic response.

By comparing Figure 6(a) and (b), we see that small absolute values of the feedback gain matrix coefficients will cause large steady-state error and slow response. Larger values will also cause the observer to be more sensitive to interfering signals. The appropriate values are those that result in small steady-state errors, which help to improve the dynamic response of observation and reduce noise sensitivity. Accordingly, the values of the parameter $l_1$ and $l_2$ are chosen to be –150.

### *Dynamic Torque Tuning Function*

Using the output of the first-order disturbance observer, combined with the knowledge that the derivative of the adhesion coefficient of the peak point is zero, a PI regulator is normally used. Under different rail conditions, however, unsuitable PI parameters can lead to skidding or slipping. It is difficult to find parameters that meet all rail conditions.

To solve this problem and improve the system's robustness, we used an additional dynamic torque tuning function $\Delta T_C$, which is combined with reasonable selection of the parameters of the PI regulator. The regulation method of the tuning function is shown in Figure 7 and is described as follows:

- First, define a reference slip velocity $v_{s\_ref}$ on the basis of the related adhesion test criteria and adhesion control experiences.
- Second, set two equidistant sidebands of slip velocity $\Delta v_s$, then the actual slip velocity $v_s$ must be controlled within the range of $[v_{s\_ref} - \Delta v_s, v_{s\_ref} + \Delta v_s]$. At time t1, if $v_s$ is lower than the range and $\dot{\mu}$ is less than zero, the operating point will move far away from the peak point. Though the operating point is in the stable region, the adhesion efficiency is too small. So $\Delta T_C$ increases at a preset rate until it reaches its upper limit $T_{ad-C1}$ to achieve higher adhesion efficiency. Otherwise, at time t4, if $v_s$ is larger than the range and $\dot{\mu}$ is less than zero, the operating point has gone through the peak point into the unstable region. For this occasion, $\Delta T_C$ has to decrease at a preset rate until it reaches its lower limit

$$\begin{cases} \begin{bmatrix} \dot{z}_1 \\ \dot{z}_2 \end{bmatrix} = \begin{bmatrix} 0 & l_1/J_{em} \\ 1 & l_2/J_{em} \end{bmatrix} \begin{bmatrix} z_1 \\ z_2 \end{bmatrix} + \begin{bmatrix} l_1 l_2/J_{em} \\ l_1 + l_2^2/J_{em} \end{bmatrix} \omega_m + \begin{bmatrix} -l_1/J_{em} \\ -l_2/J_{em} \end{bmatrix} T_e \\ \begin{bmatrix} \dot{\hat{T}}_L \\ \dot{\hat{T}}_L \end{bmatrix} = \begin{bmatrix} 1 & 0 \\ 0 & 1 \end{bmatrix} \begin{bmatrix} z_1 \\ z_2 \end{bmatrix} + \begin{bmatrix} l_1 \\ l_2 \end{bmatrix} \omega_m. \end{cases} \tag{13}$$

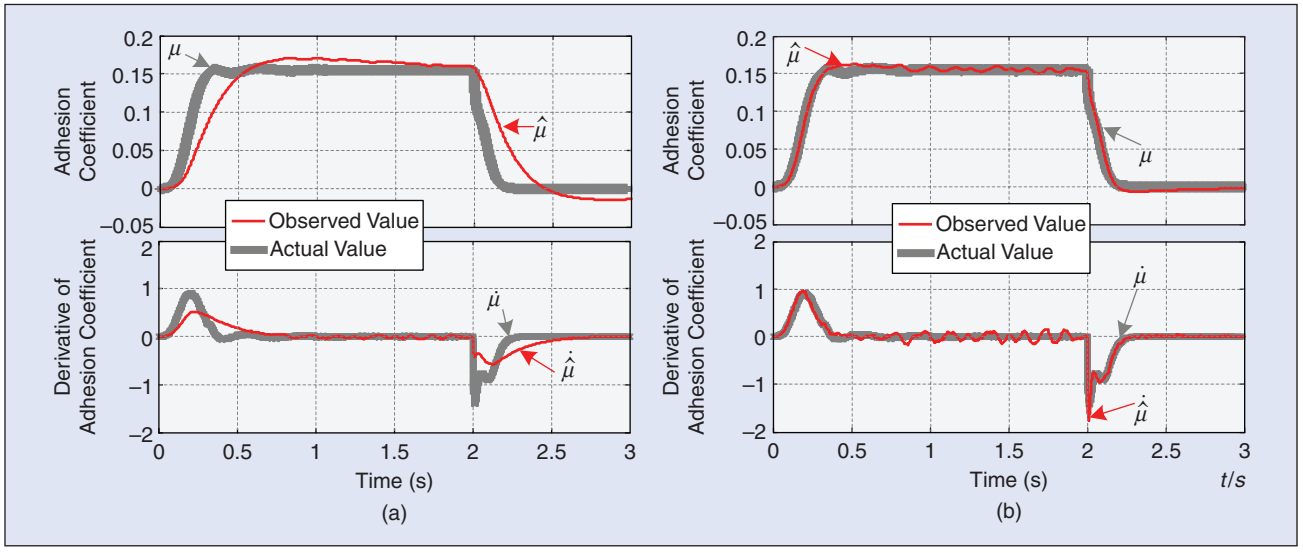


FIGURE 6 – The simulation results of first-order disturbance observer with (a) $l_1 = l_2 = -30$ and (b) $l_1 = l_2 = -150$.

$-T_{\text{ad}-C2}$. For both occasions, $\Delta T_C$ will recover to zero with another slope when $v_s$ is back to the range.

- Third, $\mu$ will increase when the operation point moves toward the peak point due to the characteristics of the adhesion curve in Figure 4, i.e., $\dot{\mu}$ will be greater than zero during the movement. This characteristic can be used to achieve a real-time correction of $v_{s\_\text{ref}}$. For example, at time [t2, t3], when $\Delta T_C$ reaches its upper limit $T_{\text{ad}-C1}$ and $\dot{\mu}$ is larger than zero, there is still more space for larger $v_{s\_\text{ref}}$, and it could be increased to approach higher adhesion efficiency.

The auxiliary tuning torque $\Delta T_C$ can help the PI regulator track much higher adhesion efficiency under uncertain rail conditions, which also prevents the operating point from back adjustment or moving to the unstable region and effectively improves the system's robustness.

### *Traction Control Using the Proposed Adhesion Controller*

The traction control system combined with the proposed adhesion controller is shown in Figure 8, where the reference vehicle velocity $v_t$ can be calculated from (14). In the figure, the final torque reference input to the FOC strategy is calculated through two parts: general vehicle logic control and the proposed adhesion control

$$\begin{cases} v_t = \min(v_{d1} \ldots v_{d4}, v_T) \\ \quad \text{when powering} \\ v_t = \max(v_{d1} \ldots v_{d4}, v_T) \\ \quad \text{when braking} \\ \omega_m = \text{ave}(v_{d1} \ldots v_{d4}) R_g / r \\ T_{\text{ref}} = \min(T_{\text{limit}}, T_{\text{ad}}). \end{cases} \quad (14)$$

The general vehicle logic control is used to produce the effective torque command value $T_{\text{limit}}$, which is first derived from the handle and traction characteristics. Then the states of the entire traction system, such as the temperature coefficients of the heat-sink, motors, filter, and air, the wheel diameter differences, and the weight change, will also limit the amplitude of the reference torque. After that, the jerk control, which is used to control passenger comfort, will regulate the change rate of the torque.

Meanwhile, in the proposed adhesion control, the observed motor torque from the FOC algorithm and the equivalent wheel speed $\omega_m$ in (14) are used as the input signal for the first-order disturbance observer, which is proposed to obtain the derivative value, $\dot{T}_L$, of the current traction condition. Then the PI regulator combined with auxiliary torque tuning, $\Delta T_C$, outputs the final available torque reference $T_{\text{ad}}$.

In a general traction calculation of the traction system design, the adopted adhesion coefficient is normally less than the available maximum value. Therefore, under good wheel-rail surface conditions, $T_{\text{ad}}$ is usually greater than $T_{\text{limit}}$, and $T_{\text{limit}}$ is chosen to meet the traction demand. When the rail conditions worsen, however, the available adhesion coefficient

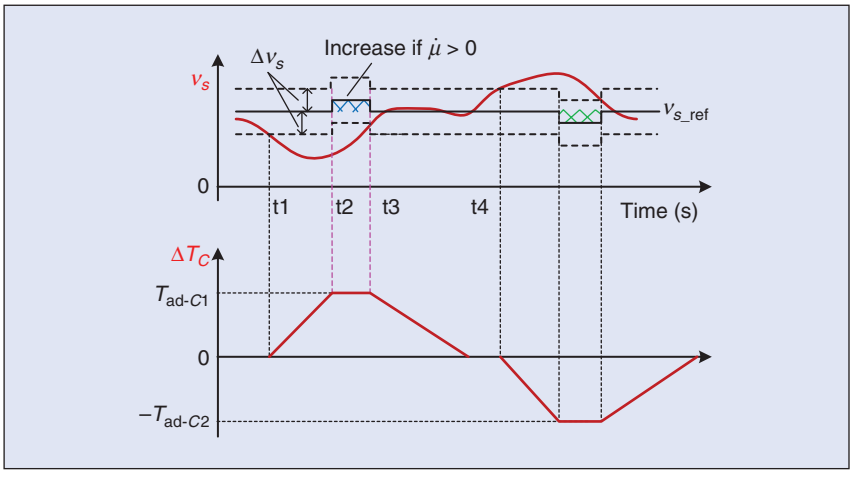


FIGURE 7 – An illustration of auxiliary dynamic torque tuning.

**In a general traction calculation of the traction system design, the adopted adhesion coefficient is normally less than the available maximum value.**

is greatly reduced and may result in $T_{ad}$ less than $T_{limit}$, at which point $T_{ad}$ should be chosen as the final reference torque to avoid heavy adhesion problems. Thus, the final torque reference $T_{ref}$ can be selected according to (14).

## Simulation and Line Experimental Verification

To verify the proposed adhesion control strategy, a vehicle dynamic model was built in MATLAB/Simulink for simulation verification. Then, self-research traction converters for a type A metro vehicle of Guangzhou Subway Line 1 were used for the onsite line experimental validation. The vehicle consists of four powered carriages and two trailer carriages, and each powered carriage has four traction motors that are driven by two traction converter models, respectively. The parameters of the vehicle are given in Table 1.

### *Simulation Analysis*

Figure 9 shows simulation results for the conventional correction method and the proposed method, respectively. For both simulations, the vehicle accelerates under road conditions changing from dry to wet and then back to dry. The wheel-rail surface state mutates at 2 s, and the maximum available adhesion coefficient decreases, which makes the effective torque command $T_{limit}$ exceed the maximum available traction torque under the current rail condition. Therefore, the adhesion controller is activated rapidly to correct the output torque command by choosing $T_{ad}$ as the final torque command, i.e., $T_{ref} = T_{ad}$. At the same time, the controller continues to search for the adhesion peak point of the current wet rail condition, making the system operating point move gradually to the peak point.

By the conventional combination correction control, the torque reduces to 50% when slippage happens, or even to 20% when heavy slippage happens, then gradually increases to 80%, and finally to 100% of the torque command. The correction time is long, and the maximum slip velocity $v_s$ is about 2 km/h; the value of acceleration is obviously reduced.

In the proposed method, the adhesion efficiency is much higher. The zoom-in waveform of the equivalent actual $\hat{\mu}$ from time 1.95 to 2.05 s demonstrates the automatic high adhesion regulation process. Further analysis shows that the equivalent wheel line speed does not exhibit the spurt phenomenon when the wheel is on a wet rail and $v_s$ is always maintained at approximately 1 km/h. When the rail condition becomes dry at 3 s, the controller will automatically search for the adhesion peak point, and the operating point gradually moves toward to the condition of $T_{ref} = T_{limit} < T_{ad}$.

Figure 10 illustrates the simulation results of an acceleration slip phenomenon controlled by PI regulation only or by the combined torque tuning function. Figure 10(a) shows that the slip can be effectively controlled by the PI regulator, although the slip velocity remains at a high value and the actual adhesion coefficient is kept at a low level, which makes the adhesion efficiency quite low. Comparatively, when the torque tuning function is added, Figure 10(b) shows that $\Delta T_C$ is activated to reduce the output torque when $v_s$ is over the sideband range and the derivative of $\hat{\mu}$ is lower than zero; then, $\Delta T_C$ will gradually recover to zero when $v_s$ goes back to the sideband range. It can be seen that $v_s$ is controlled to a relatively lower level, and adhesion efficiency is much higher than that of Figure 10(a). Moreover, the slope of $\Delta T_C$ plays an important role on the robustness of the torque tuning: the tuning dynamic and adhesion

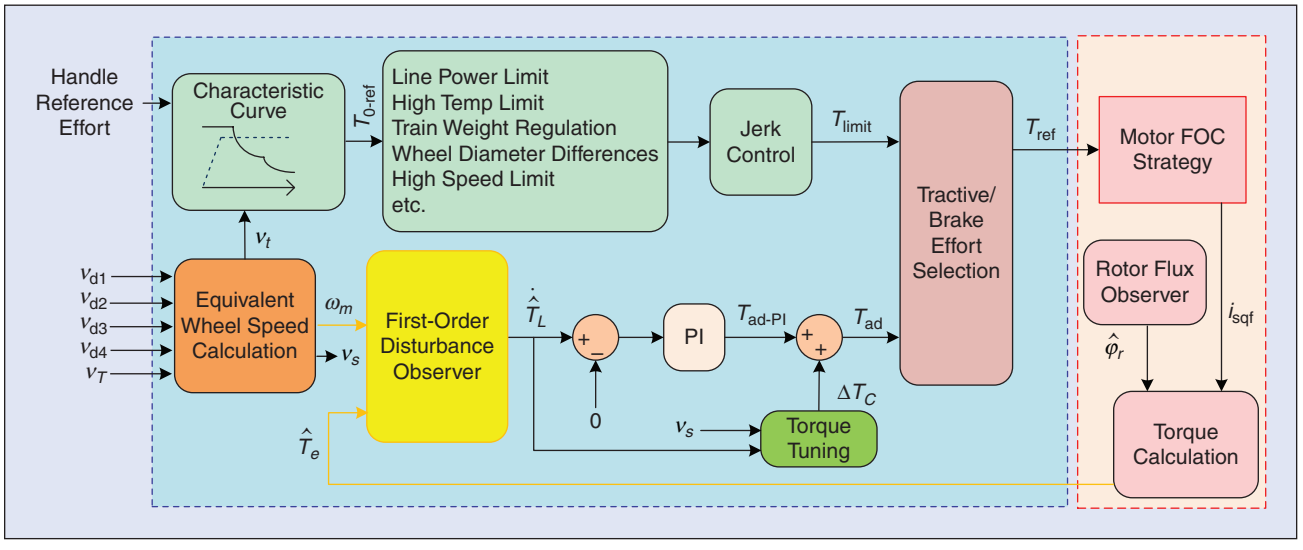


FIGURE 8 – Traction control with the proposed adhesion control strategy.

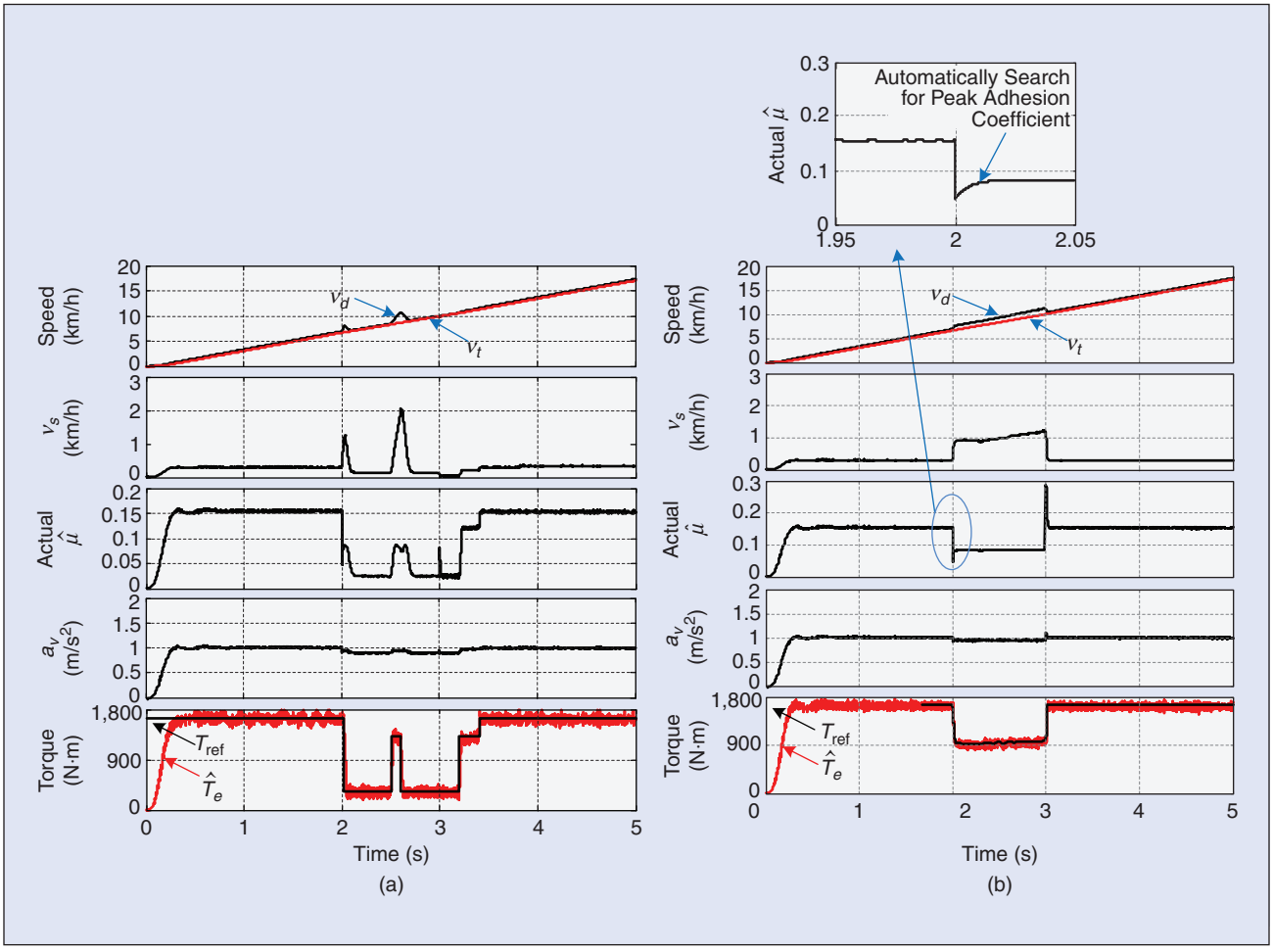


FIGURE 9 – Adhesion control simulations of the acceleration process with (a) the conventional correction method and (b) the proposed method.

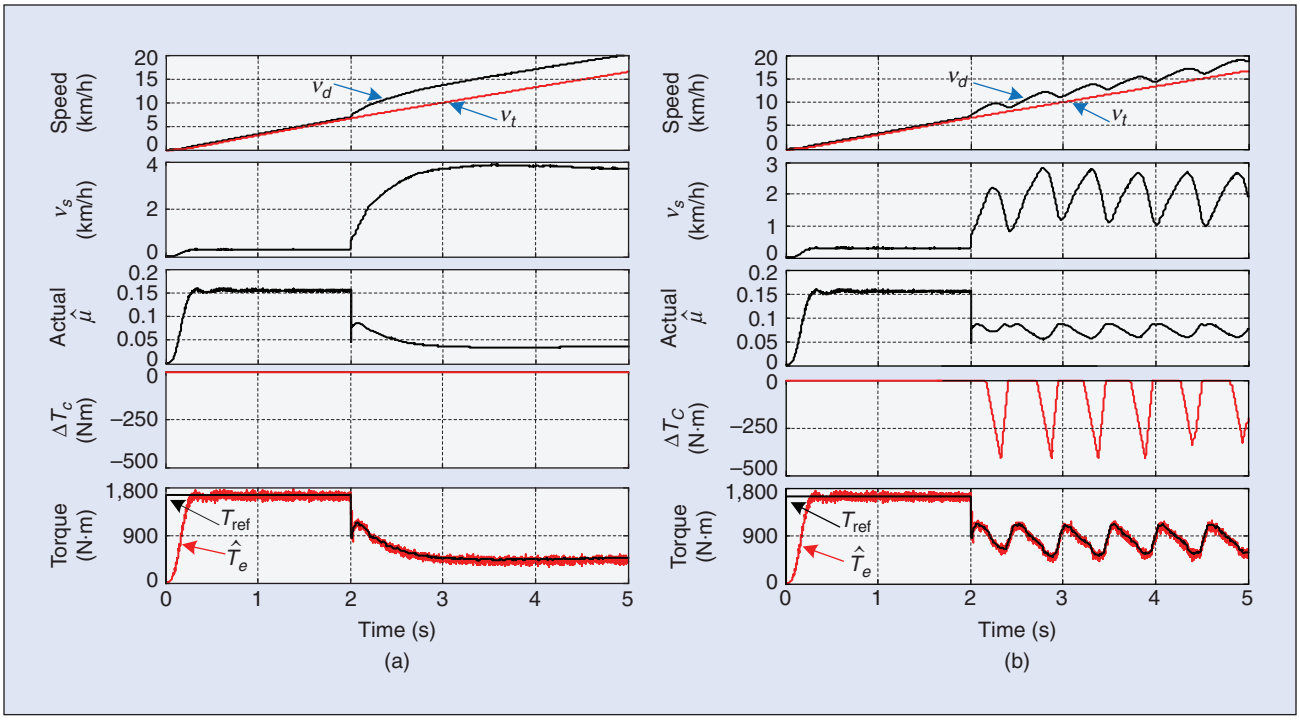


FIGURE 10 – Simulation results of adhesion control by (a) PI regulator only and (b) PI regulator combined with dynamic torque tuning.

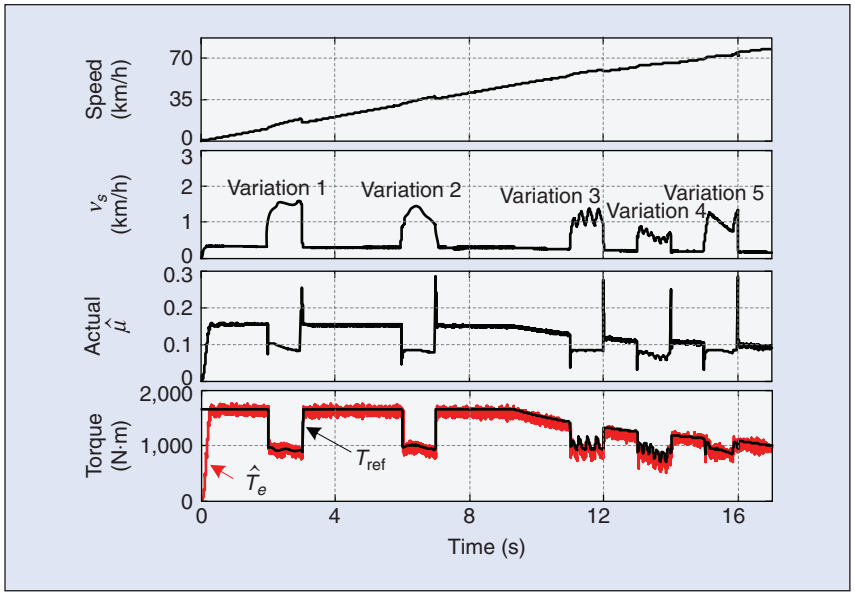


FIGURE 11 – Simulation results of a whole speed range under variable conditions.

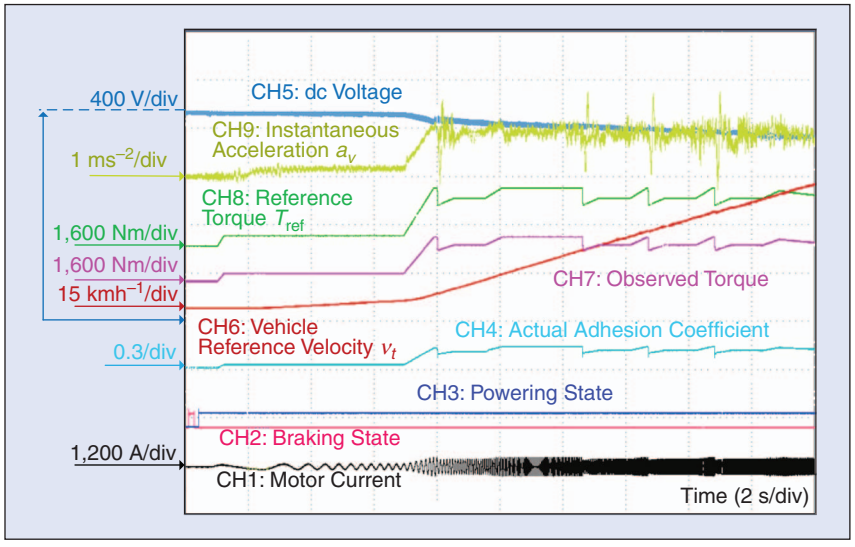


FIGURE 12 – Adhesion test results during slippage when operating in the powering state.

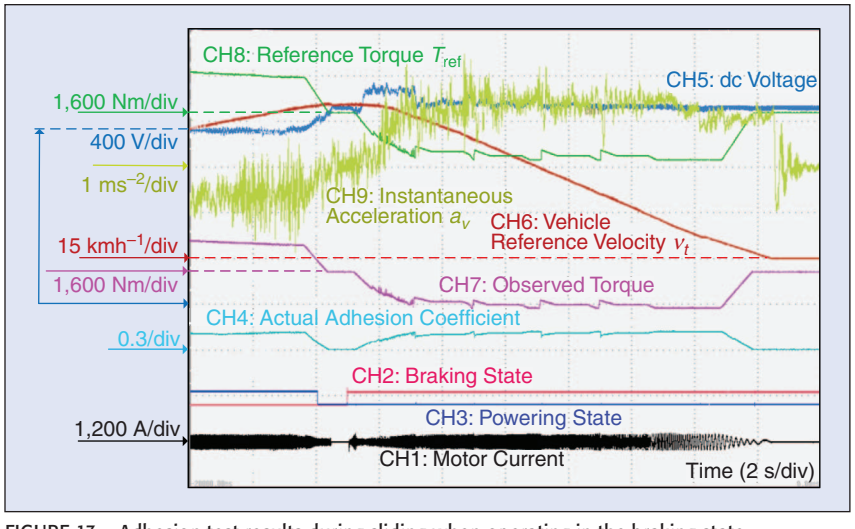


FIGURE 13 – Adhesion test results during sliding when operating in the braking state.

efficiency will be better when the slop is somewhat large under poor adhesion conditions, but the torque will fluctuate if there is no sideband and the slope is too large. This study used a slope of 1,250 Nm/s.

By using the given dynamic vehicle model, Figure 11 shows the control performance over the entire speed range under varying rail conditions, where the traction motor changes from the constant torque zone, to the constant power zone, and to the natural zone. The simulation waveforms demonstrate that the adhesion controller using the proposed strategies will be activated to prevent heavy slippage and achieve high adhesion efficiency.

### *Line Experimental Verification*

To verify the adhesion control performance in practice, an onsite test was carried out on the Guangzhou Subway Line 1. According to the metro user's demands for a traction system-type test, the adhesion test must be done during the horizontal straight line test under no-load conditions with 100% traction and braking force, and the maximum speed level must be not higher than 50 km/h on the test line. To simulate the slippage conditions on the dry rails, a liquid mixture of detergent and water was sprayed on the wheel-rail surface in front of the motor bogie wheel. The test waveforms under powering and braking states are shown in Figure 12 and Figure 13, respectively. Both results have been converted to one traction motor.

When slippage or sliding occurred, the adhesion controller reduced the torque reference $T_{ref}$ (CH8), and the observed electromagnetic torque $\hat{T}_e$ (CH7) tracked with the reference value very closely, which indicates good performance of FOC algorithm. The proposed first-order disturbance observer estimated the load torque and calculated the actual adhesion coefficient $\hat{\mu}$ (CH4) of the actual wheel-rail surface condition. Then the torque and the adhesion coefficient recovered to the maximum reference values quickly when slippage or sliding stopped. Meanwhile, the measured instantaneous acceleration $a_v$ (CH9)

changed dramatically when the adhesion problem happened, but the system remained stable overall. Meanwhile, the motor current (CH1), dc voltage (CH5), and vehicle speed (CH6) remained stable and did not exceed any of the protection limits of the traction motor drive. The controller achieved good traction and high dynamic adhesion performance.

According to the relevant International Union of Railway (UIC) standard, during slip tests, the instantaneous slide value for the wheelsets of the brake system shall not exceed 30 km/h for more than 3 s [36]. Until now, there has not been a specific standard for slip protection for traction converters, and the criterion typically adopted for the traction converter is that the slip speed must be below 5 km/h during slip tests. Additionally, the adhesion efficiency $\eta_{ad}$ calculated by the following equation can also be adopted to indirectly evaluate adhesion performance, where the control efficiency must not fall below 80%:

$$\eta_{ad} = 100\% \times \int_{t1}^{t2} a_{measured} \Big/ \int_{t1}^{t2} a_{fictitious}, \quad (15)$$

where $a_{measured}$ is the measured acceleration within the slide or slip period [t1, t2] and $a_{fictitious}$ is a fictitious acceleration, which is calculated from the total reference force divided by the total mass of the vehicle.

The adhesion efficiencies of the simulation results in Figure 9 and the test results can be calculated by using (15); these are shown and compared in Table 2, where the onsite line test control efficiency of the conventional adhesion method is obtained from our previous test. From the table, it can be seen that the adhesion efficiency of the proposed method has improved significantly when compared with the conventional method.

**The simulation waveforms demonstrate that the adhesion controller using the proposed strategies will be activated to prevent heavy slippage and achieve high adhesion efficiency.**

From the simulation and experiments, we have validated the good performance of the proposed adhesion control method; the merits of this method include high dynamic response to varying rail surface conditions, immunity to interference, and easy modeling and engineering usage. The single-axle model, however, makes several simplifying assumptions. There will also be some limitations when parallel motors are used, e.g., the observed torque of the parallel motors may not be distributed equally among motor axles when the difference in wheel diameters reaches a large value, because not all of the motor axles can reach the highest adhesion utilization. In the one-converter/one-motor driving mode, however, such as in an independent-wheel tram or in rolling stock, this issue does not arise.

## Conclusions

The main focus of this article is on an adhesion control strategy for urban railway vehicles utilizing a disturbance observer, combined with an additional dynamic torque tuning function, which was adopted to adjust the motor torque command after the PI controller. This tuning function helps compensate for the drawback of the PI controller and improves the control robustness under different rail conditions. This strategy prevents heavy wheel slippage and achieves high adhesion efficiency. Simulation and line experimental results are carried out by using practical vehicle and traction converters, and the results show good slippage regulation and robustness under different rail conditions. The proposed adhesion control method has a good dynamic response under varying rail surface conditions, it is immune to interference, and it is easy for modeling and implementation. The method can also be easily extended to other railway vehicles, such as mainline railways and rubber-tire trains.

**TABLE 2 – ADHESION CONTROL EFFICIENCY COMPARISON.**

| SIMULATION ADHESION EFFICIENCY | | EXPERIMENT ADHESION EFFICIENCY | | |
|---|---|---|---|---|
| Figure 9(a) | Figure 9(b) | Conventional method | Traction Figure 12 | Brake Figure 13 |
| 85.2% | 92.6% | 86.2% | 91.7% | 92.9% |


## Acknowledgment

This work was supported in part by the National Natural Science Foundation of China (U1134204) and the China National Science and Technology Support Program (2013BAG21Q00 and 2015BAG13B01). The authors would like to thank the engineers of Guangzhou Metro and Beijing Qiansiyu Electric Co., Ltd., for their valuable cooperation during onsite testing. The authors would also like to thank the China Scholarship Council.


## Biographies


***Lijun Diao*** (ljdiao@bjtu.edu.cn) received his Ph.D. degree in electrical engineering from Beijing Jiaotong University, China, in 2008. He was a postdoctoral researcher in the Department of Traffic Transportation Engineering at the same university from 2008 to 2010. He has been an associate professor with the School of Electrical Engineering, Beijing Jiaotong University, since 2013. He was also an academic visitor in the Faculty of Engineering and Environment at the University of Southampton, United Kingdom, from 2016 to 2017. His research interests include power electronics and ac drives, transportation electrification applications, and safety control. He is a Member of the IEEE.

***Leiting Zhao*** (zhaoleiting@zemt.cn) received his Ph.D. degree from Beijing Jiaotong University, China, in 2014. He has worked as a software engineer at the China Academy of Railway Sciences since 2015. His research interests include the design and control of motor drives, DSP applications, and applications of optimization techniques in control systems.

***Zheming Jin*** (zhe@et.aau.dk) received his B.Sc. and M.Sc. degrees from Beijing Jiaotong University, China, in 2013 and 2015, respectively. He is currently working toward his Ph.D. degree in the Department of Energy Technology, Aalborg University, Denmark. His current research interests include power electronics, energy storage for microgrids and transportation electrification, dc distribution systems, and dc microgrids. He is a Student Member of the IEEE and the IEEE Industrial Electronics Society.

***Lei Wang*** (leiwang@bjtu.edu.cn) received his Ph.D. degree in electrical engineering from Beijing Jiaotong University, China in 2010. He worked as a postdoctoral researcher with the Institute of Electrical Engineering, Chinese Academy of Sciences, from 2010 to 2012. He is now a lecturer in the School of Electrical Engineering, Beijing Jiaotong University. His research interests focus on the control and life prediction of large-capacity power electrical equipment. He is a Member of the IEEE.

***Suleiman M. Sharkh*** (S.M.Abu-Sharkh@soton.ac.uk) received his Ph.D. degree in electrical engineering from the University of Southampton, United Kingdom, in 1994. He is currently the head of the Mechatronics Engineering Group at the University of Southampton and professor of power electronics, machines, and drives. His research interests include high-performance electrical machines and power electronics for demanding applications. He was the winner of the Faraday SPARKS Award in 2002 and the Engineer Energy Innovation and Technology Award in 2008. He is a Senior Member of the IEEE.

## References


[1] Adhesion railway. [Online]. Available: https://en.wikipedia.org/wiki/Adhesion_railway

[2] H. J. Ryoo, S. J. Kim, G. H. Rim, Y. J. Kim, and M. S. Kim, "Novel anti-slip/slide control algorithm for Korean high-speed train," in *Proc. 29th Annu. Conf. IEEE Industrial Electronics Society, Roanoke*, Nov. 2–6, 2003, vol. 3, pp. 2570–2574.

[3] K. Nagase, N. Tagawa, E. Maebashi, H. Nomoto, and K. Okikura, "The realities of adhesion between rail wheels on main line (result of the survey by slipping adhesive bogie)," in *Proc. Japan Society of Mechanical Engineers*, vol. 504, pp. 282–286, Aug. 1988.

[4] S. Shirai, "Adhesion phenomena at high-speed range and performance of an improved slip-detector," Railway Technical Research Institute, Kokubunji, Japan, Quarterly Rep., 1977, pp. 189–190.

[5] I. P. Isaev and A. L. Golubenko, "Improving experimental research into the adhesion of the locomotive wheel with the rail," *Rail Int.*, vol. 20, no. 8/9, 1989.

[6] T. Ohyama, "Some basic studies on the influence of surface contamination on adhesion force between wheel and rail at higher speeds," Railway Technical Research Institute, Kokubunji, Japan, Quarterly Rep., 1989.

[7] T. Watanabe and M. Yamashita, "Basic study of anti-slip control without speed sensor for multiple motor drive of electric railway vehicles," in *Proc. Conf. Power Conversion*, Osaka, 2002, vol. 3, pp. 1026–1032.

[8] J. W. Finch and D. Giaouris, "Controlled AC electrical drives," *IEEE Trans. Ind. Electron.*, vol. 55, no. 2, pp. 481–491, Feb. 2008.

[9] B. Allotta, E. Meli, A. Ridolfi, and A. Rindi, "Development of an innovative wheel–rail contact model for the analysis of degraded adhesion in railway systems," *Tribology Int.*, vol. 69, pp. 128–140, Jan. 2014.

[10] O. Polach, "Creep forces in simulations of traction vehicles running on adhesion limit," *Wear*, vol. 258, pp. 992–1000, Mar. 2005.

[11] E. Meli and A. Ridolfi, "An innovative wheel–rail contact model for railway vehicles under degraded adhesion conditions," *Multibody System Dynamics*, vol. 33, no. 3, pp. 285–313, Mar. 2015.

[12] Institution of Civil Engineers. *Urban Railways and the Civil Engineer.* London: Thomas Telford, 1988.

[13] R. de Castro, R. E. Araujo, and D. Freitas, "Wheel slip control of EVs based on sliding mode technique with conditional integrators," *IEEE Trans. Ind. Electron.*, vol. 60, no. 8, pp. 3256–3271, Aug. 2013.

[14] N. Mutoh, "Driving and braking torque distribution methods for front- and rear-wheel-independent drive-type electric vehicles on roads with low friction coefficient," *IEEE Trans. Ind. Electron.*, vol. 59, no. 10, pp. 3919–3933, Oct. 2012.

[15] W. Y. Wang, I.-H. Li, C. P. Tsai, S. F. Su, and S. B. Hsu, "Dynamic slip-ratio estimation and control of antilock braking systems using an observer-based direct adaptive fuzzy–neural controller," *IEEE Trans. Ind. Electron.*, vol. 56, no. 5, pp. 1746–1756, May 2009.

[16] A. Horie, T. Mizobuchi, and K. Nakamura, "Efficient train traction system that reduces maintenance work," *Hitachi Rev.*, vol. 48, pp. 139–143, Mar. 1999.

[17] D. Y. Park, M. S. Kim, D. H. Hwang, J. H. Lee, and Y. J. Kim, "Hybrid re-adhesion control method for traction system of high-speed railway," in *5th Conf. Electrical Machines and Systems*, 2001, vol. 2, pp. 739–742.

[18] D.-H. Hwang, M.-S. Kim, D.-Y. Park, Y.-J. Kim, and D.-H. Kim, "Re-adhesion control for high-speed electric railway with parallel motor control system," in *Proc. IEEE Int. Symp. Industrial Electronics*, 2001, vol. 2, pp. 1124–1129.

[19] H. Yamazaki, Y. Karino, T. Kamada, M. Nagai, and T. Kimura, "Effect of wheel-slip prevention based on sliding mode control theory for railway vehicles," *Vehicle System Dynamics*, vol. 46, pp. 255–270, Apr. 2008.

[20] F. Kock and M. Weinhardt, "Tractive effort and wheel slip control of locomotive type 120," in *Proc. Conf. Tenth World Congr. Automatic Control*, Munich, West Germany, 1987, vol. 3, pp. 259–267.

[21] P. Escane, D. M. Pietrzak, and B. de Fornel, "Optimisation of a railway traction system drive control vs. slip perturbation," in *Proc. IEEE Conf. Industry Applications*, Rome, Italy, 2000, vol. 3, pp. 1909–1916.

[22] Y. Matsumoto, N. Eguchi, and A. Kawamura, "Novel re-adhesion control for train traction system of the 'Shinkansen' with the estimation of wheel-to-rail adhesion force," in *Proc. IEEE 27th Annu. Conf. Industrial Electronics Society*, Denver, Colorado, 2001, vol. 2, pp. 1207–1212.

[23] K. Yuki, T. Hemmi, T. Hasebe, I. Yasuoka, K. Kondo, and K. Matsuoka, "Application of speed sensorless control to railway traction field," in *Proc. Conf. IEEE Power Conversion*, Osaka, Japan, 2002, vol. 3, pp. 1033–1038.

[24] M. Yamashita and T. Watanbe, "A re-adhesion control method without speed sensor for electric railway vehicles," in *Proc. Conf. IEEE Electric Machines and Drives*, Madison, WI, 2003, vol. 1, pp. 291–296.

[25] S. K. Kwon, U. Y. Huh, H. I. Kim, I. Yasuoka, K. Kondo, K. Matsuoka. "Re-adhesion control with estimated adhesion force coefficient for wheeled robot using fuzzy logic," in *Proc. IEEE 30th Annu. Conf. Industrial Electronics Society*, Busan, South Korea, 2004, vol. 3, pp. 2530–2535.

[26] J. Huang, J. Xiao, Y. F. Bai, S. Q. Liao. "Optimized adhesion control of electric locomotives based on wavelet analysis and cloud model," in *Proc. Conf. Transportation Engineering*, 2007, pp. 3209–3214.

[27] K. Ohishi, S. Kadowaki, Y. Smizu, T. Sano, S. Yasukawa, and T. Koseki, "Anti-slip readhesion control of electric commuter train based on disturbance observer considering bogie dynamics," in *Proc. Conf. IEEE Industrial Electronics*, Nov. 6–10, 2006, pp. 5270–5275.

[28] S. Kadowaki, K. Ohishi, T. Hata, N. Iida, M. Takagi, T. Sano, and S. Yasukawa, "Antislip readhesion control based on speed-sensorless vector control and disturbance observer for electric commuter train: Series 205-5000 of the East Japan Railway Company," *IEEE Trans. Ind. Electron.*, vol. 54, pp. 2001–2008, Aug. 2007.

[29] S. Kadowaki, K. Ohishi, I. Miyashita, and S. Yasukawa, "Re-adhesion control of electric motor coach based on disturbance observer and sensor-less vector control," in *Proc. Conf. Power Conversion*, Osaka, Japan, 2002, vol. 3, pp. 1020–1025.

[30] W. L. Lin, L. T. Zhao, and K. Dong, "Performance analysis of re-adhesion optimization control based on full-dimension state observer," *Procedia Eng.*, vol. 23, pp. 531–536, Dec. 2011.

[31] K. Imai, K. Ohishi, T. Sano, S. Makishima, and S. Yasukawa, "Real-time distribution control of torque reference of commuter train for fine re-adhesion contol," in *Proc. 11th IEEE Int. Workshop Advanced Motion Control*, Nagaoka, Japan, 2010, pp. 228–233.

[32] S. Andreas, *Electric Traction—Motion Power and Energy Supply: Basics and Practical Experience.* 2nd ed. Munich: Oldenbourg Industrieverlag GmbH, 2014, p. 46.

[33] W. L. Lin, "Metro traction drive system modeling, macro design and engineering optimization (in Chinese)." Ph.D. dissertation, Beijing Jiaotong University, Beijing, China, 2010.

[34] B. K. Bose, *Modern Power Electronics and AC Drives.* Beijing, China: China Machine Press, 2005.

[35] H. P. Sung, S. K. Jong, J. C. Jeong, and H. O. Yamazaki, "Modeling and control of adhesion force in railway rolling stocks," *IEEE Trans. Control Syst.*, vol. 28, pp. 44–58, Oct. 2008.

[36] *Brakes—Specifications for the Construction of Various Brake Parts—Wheel Slide Protection Device (WSP)*, Union Internationale des Chemins de Fer Standard UIC541-05-2005.